Journal of Alloys and Compounds 615 (2014) S437–S443

Contents lists available at ScienceDirect

Journal of Alloys and Compounds

journal homepage: www.elsevier.com/locate/jalcom

Optimal conditions for the deposition of novel anticorrosive coatings by RF magnetron sputtering for aluminum alloy AA6082

S.B. Brachetti-Sibaja [a,b], M.A. Domínguez-Crespo [c,*], S.E. Rodil [d], A.M. Torres-Huerta [c]

[a] Instituto Politécnico Nacional, Postgraduate Student of CICATA-Unidad Altamira, Mexico
[b] Instituto Tecnológico de Cd. Madero, Cd. Madero, Tamaulipas, Mexico
[c] CICATA-Altamira, Instituto Politécnico Nacional, IPN Km 14.5 Carretera Tampico-Puerto Industrial Altamira, C.P. 89600 Altamira, Tamaulipas, Mexico
[d] Universidad Nacional Autónoma de México, IIM, D.F., Mexico

ARTICLE INFO

Article history:
Available online 2 February 2014

Keywords:
RF magnetron sputtering
AA6082 aluminum alloy
Rare earths
Coatings
Corrosion resistance

ABSTRACT

Cerium and lanthanum coatings were deposited on glass, silicon (100), and aluminum alloy by RF magnetron sputtering in which several experimental conditions such as power, substrate temperature, and deposition time were varied, using pure CeO_2 and La_2O_3 targets. The effect of deposition parameters on the bonding structure, surface morphology and properties against corrosion of rare earth (RE) coatings formed on metallic substrate was reported. The microstructure and chemistry of the thin film were characterized by X-ray diffraction (XRD), Scanning Electron Microscopy (SEM), and X-ray photoelectron spectroscopy (XPS); whereas their use as corrosion resistant coatings was studied in aqueous NaCl solution (3.0 wt%) by using polarization curves. Variations in these properties were observed by increasing the substrate temperature which modifies the crystallinity of the rare earth coatings. XRD and XPS findings indicate that the cerium coatings are composed by CeO_2 and a significant quantity of Ce_2O_3 due to oxygen deficiency in the sputtering chamber, whereas $La_2O_3/La(OH)_3$ and some La intermetallic compounds are detected in the lanthanum films. Variations in the E_{corr} and I_{corr} were found as a function of the thickness, texture, and morphology of the as-prepared coatings.

1. Introduction

The corrosion of metallic structures has a significant impact on the economies of countries. Hence, a big effort is made every year to overcome its effects. Most high strength aluminum alloys used in aircraft and machining industries are susceptible to pitting corrosion [1], inter-granular corrosion [2], and stress corrosion cracking [3]. For decades, the corrosion protection of aluminum alloys relied on highly effective hexavalent chromium compounds to form conversion coatings [4] or corrosion inhibitor pigments in epoxy primer coatings [5]. However, the high toxicity of these chromium compounds has limited their use [6]. Coatings containing rare earth (RE) ions, such as cerium or lanthanum [7], constitute an interesting alternative to eliminate traditional chromium compounds because of their good self-healing properties and low environmental impact [8]. However, some limitations of RE coatings obtained by conventional methods are: (i) the precipitation of an insoluble protective Ce oxide/hydroxide layer that produces coatings with irregular characteristics; (ii) the presence of cracks that can penetrate the entire cross-section of the layer. These cracks represent preferential pathways to attack the substrate by aggressive corrosive species. For this reason, the development of new environmentally friendly protective coatings to enhance the anticorrosive properties of materials is of great research interest. Using physical vapour deposition processes, simple coatings that consist of only one phase, or of multiple layers, and coatings with a gradient composition within the layer [9], can be deposited at sufficiently low substrate temperatures [10]. To our knowledge, there are few reports of the use of sputtered Ce and La oxide coatings to protect aluminum alloys against corrosion.

The results reported in this paper are a consequence of research sponsored by the National Council of Science and Technology of Mexico (CONACYT) to study the anticorrosive properties of sputtered rare earth coatings and to develop new alternatives to improve the corrosion resistance of aluminum alloys. Specifically, this study aims to investigate the effect of sputtering power, substrate temperature and deposition time on the bonding structure, surface morphology and corrosion resistance of deposited CeO_2 and La_2O_3 films formed on AA6082 aluminum alloy using a RF magnetron sputtering.

* Corresponding author.
E-mail address: mdominguezc@ipn.mx (M.A. Domínguez-Crespo).

http://dx.doi.org/10.1016/j.jallcom.2014.01.195
0925-8388/

2. Experimental procedure

Aluminum alloy 6082 plates with a thickness of 10 mm, were cut into 2 × 2 and 1 × 1 cm^2 pieces and used as substrates. Prior to deposition, the substrates were finely abraded using 1000, 1500, and 2000 grade SiC paper, cleaned by rinsing with deionized water, and finally, by sonication in isopropyl alcohol and deionized water for 20 min, respectively.

The rare earth oxides films were deposited using an RF magnetron sputtering system built in our laboratory. CeO_2 and La_2O_3 targets (99.99% purity, 2″ in diameter with copper bonding, Plasmaterials) were used in an Ar atmosphere of ultra-high purity with a gas flow of 30 sccm. The equipment has an automated gas flow system that keeps the deposition pressure constant. The chamber pressure was 20 m Torr (266.45 m Pa) and the substrate to target distance was 6 cm. Two RF sputtering power were used, 60 and 90 W (P). The rare earth coatings were deposited at each power using two different substrate temperatures (*T*, 80 and 200 °C) and three different deposition times (*t*, 25, 40, and 60 min). The coatings were simultaneously deposited onto glass and silicon (1 0 0) substrates, which were chosen for analytical purposes.

The phase composition and crystal structure of as-synthesized films were determined by powder X-ray diffraction using an Advanced Bruker D8 diffractometer, with Cu Kα radiation at 35 kV, 25 mA, and a scan rate of 0.021 min^{-1}. Film morphology was examined by scanning electron microscopy using a JEOL JSM 7600F. Thickness of films deposited on silicon (1 0 0) substrates were examined by Spectroscopic Ellipsometry (SE, at a 70° angle of incidence) using a HORIBA JOBIN–YVON UVISEL ellipsometer. The chemical compositions of the films were characterized by X-ray Photoelectron Spectroscopy (XPS) using a commercial XPS VG Microtech Multilab ESCA 2000 with a CLAM MCD detector, Al Kα radiation ($h\upsilon$ = 1453.6 eV), operating at 8E−7 Pa, using a 500 μm spatial resolution and 50 and 20 eV pass energy for the acquisition of the survey and high resolution spectra, respectively. Curve fitting of high resolution XPS spectra acquired in the regions of the C 1s and O 1s and the La 3d and Ce 3d photoelectron peaks, respectively, for the different metal oxide films, was performed with the SDPv4.1 software® to obtain the elemental composition. The topography and roughness were analyzed and measured by an AFM, Veeco, Model diMultiMode V, controller diNanoScope V, with cantilever RTESP tips.

The corrosion behaviour of coated and uncoated aluminum alloy was determined by polarization resistance (Rp) and potentiodynamic polarization measurements. A potentiostat/galvanostat (Gamry 600 series) was used with a conventional experimental set-up of a three-electrode cell. A graphite bar (counter electrode) and a saturated calomel electrode (SCE, reference electrode) were employed to perform the corrosion experiments. The working electrode had an exposed area of 0.126 cm^2 and 3.0 wt% NaCl solutions was chosen as the corrosive medium, because the chloride ion is present in many corrosive environments. At least three replications were used for every corrosion-rate measurement. Polarization resistance (Rp) plots were conducted from 20 mV cathodic to 20 mV anodic of corrosion potential at a 0.5 mV s^{-1} sweep rate. Rp is defined as the slope at zero current on the potential versus current graph obtained from the experiment. To evaluate the susceptibility of the surface of the samples to pitting corrosion and to obtain information about the corrosion rate and corrosion potential, potentiodynamic polarization curves were scanned. These curves were measured from cathodic to anodic areas from −500 mV vs. SCE (E_{ocp}) to 1000 mV at a sweep rate of 0.5 mV s^{-1}.

3. Results and discussion

3.1. Influence of process parameters on coatings (sputtering power, substrate temperature, and deposition time)

Coating technology has evolved and developed in the last decades in different industries, using a wide range of preparation methods. Techniques such as evaporation, plating, dipping, chemical vapour deposition and spraying have been commonly used to growth thin films on different substrates however, they are somewhat limited to the melting temperature materials, and some of them are restricted only to metallic coatings. By contrast, the sputtering process has different advantages such as: deposition ranges from 1 nm s^{-1} to 10 nm s^{-1}, coating uniformity in the range of few percentage even for several meters long cathodes, deposition of large variety of film materials (nearly all metals and compounds) and easy to scale up, among others. In summary, the industrial use of this technique has let the economic manufacturing of innovative products [11]. In this manner, the major steps of the coating process can be divided in pre-treatment of the alloy surfaces prior to coating, establishing of coating deposition parameters and treatment of the coated surfaces after deposition [12].

Thus, to evaluate the protection against corrosion provided by the sputtered CeO_2 and La_2O_3 thin films, different experiments were carried out varying power, substrate temperature, and deposition time. Consequently, the diverse experiments are discussed in terms of the effect that the operating conditions have on the morphology, thickness, and/or electrochemical behaviour of the CeO_2 and La_2O_3 coatings deposited by RF magnetron sputtering on the AA6082 aluminum alloy.

The deposition parameters used to obtain the CeO_2 and La_2O_3 layers producing different roughness and thicknesses are listed in Table 1. As expected, it was observed an increase in the deposition rate, as the power increased from 60 W to 90 W, although a slight drop in the deposition rate can be seen with the substrate temperature. In addition, for fixed power and substrate temperature, the deposition time had an adverse effect on the thickness of both rare earth coatings.

AFM observations of the different samples were carried out, with the aim of comparing their surface roughness. From Table 1 and considering the mean roughness value of bare substrate (∼81 nm), it can be observed that the mean roughness also decreased with the substrate temperature, fixed power and deposition time. An explanation for the variation in both the deposition rate and mean film roughness is not clear. Perhaps, this effect could be due to re-sputtering of the films, either by a physical process or a chemical reaction. Target poisoning is another alternative, although the atmosphere was not reactive and the targets were oxides. Moreover, no drastic variations in the voltage–current characteristics were observed. Gas rarefication due to a higher amount of reactive Ce and La atoms in the gas may be another contributor. This issue requires further experiments, which are beyond the objective of this paper.

3.2. Microstructural analysis

X-ray diffraction analysis was used to identify the phases of the rare earth coatings that were formed under the different experimental conditions described in this work. Figs. 1 and 2 show the XRD patterns for the uncoated and the CeO_2- and La_2O_3-coated AA6082 aluminum alloy substrates. The XRD patterns of CeO_2 films

Table 1
Deposition parameters and correlation between the thickness and mean roughness.

Experiment	Thickness (nm)	Deposition rate (nm s^{-1})	Mean roughness (nm)
CeO_2			
$P_{60}T_{80}t_{25}$	19.29	0.012	103.51
$P_{60}T_{200}t_{25}$	12.73	8.4E−3	66.73
$P_{60}T_{80}t_{40}$	30.84	0.012	69.35
$P_{60}T_{200}t_{40}$	22.95	9.5E−3	50.52
$P_{60}T_{80}t_{60}$	32.38	8.9E−3	62.48
$P_{60}T_{200}t_{60}$	40.08	0.011	44.82
$P_{90}T_{80}t_{25}$	44.61	0.029	218.18
$P_{90}T_{200}t_{25}$	42.22	0.028	91.74
$P_{90}T_{80}t_{40}$	52.86	0.022	84.48
$P_{90}T_{200}t_{40}$	46.06	0.019	76.33
$P_{90}T_{80}t_{60}$	149.10	0.041	132.98
$P_{90}T_{200}t_{60}$	157.91	0.043	120.25
La_2O_3			
$P_{60}T_{80}t_{25}$	269.45	0.180	114.61
$P_{60}T_{200}t_{25}$	354.26	0.236	96.54
$P_{60}T_{80}t_{40}$	337.55	0.140	161.26
$P_{60}T_{200}t_{40}$	310.14	0.129	130.43
$P_{60}T_{80}t_{60}$	390.22	0.108	158.10
$P_{60}T_{200}t_{60}$	349.12	0.097	123.47
$P_{90}T_{80}t_{25}$	528.47	0.352	153.38
$P_{90}T_{200}t_{25}$	498.94	0.332	172.80
$P_{90}T_{80}t_{40}$	545.20	0.227	195.08
$P_{90}T_{200}t_{40}$	670.75	0.279	157.63
$P_{90}T_{80}t_{60}$	750.57	0.208	150.47
$P_{90}T_{200}t_{60}$	835.54	0.232	280.32

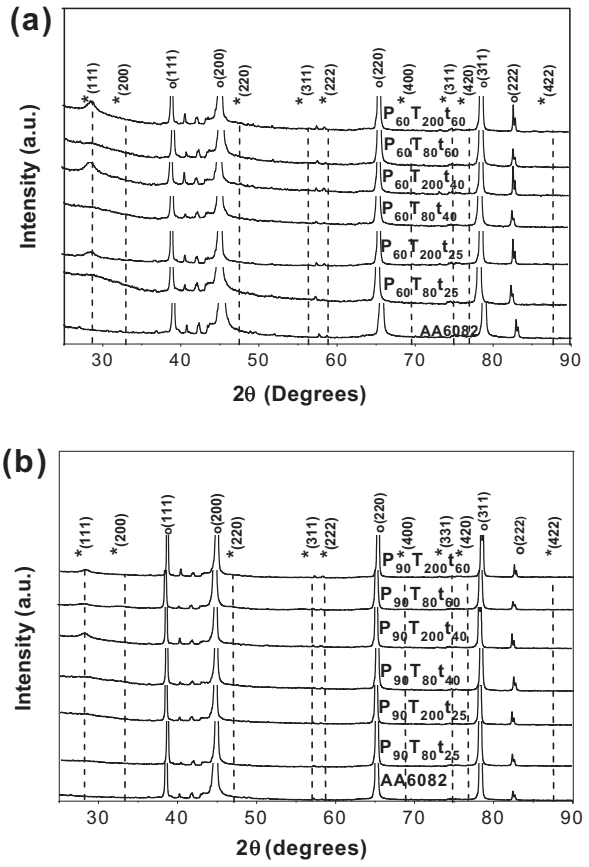

Fig. 1. X-ray diffraction patterns for CeO_2 coatings onto AA6082 using different deposition parameters: (a) 60 W and (b) 90 W.

deposited on metallic substrates indicate that CeO_2 improves the crystallinity with increasing substrate temperature and exhibit a strong tendency to grow in the (111) direction independent of applied power or deposition time (Fig. 1a and b). Therefore, the effect of sputtering power on texture appears to be non-important.

To examine the effect of substrate on film deposition, CeO_2 films were deposited on both glass and silicon (100). The results indicate that the CeO_2 films have similar crystallinity with the (111) orientation on glass and on silicon, although low intensity peaks of Ce_2O_3 (510) are also observed, formed with low oxygen content. In comparison, the XRD patterns of sputtered lanthanum oxide coatings are shown in Fig. 2a and b. For all spectra, the peaks at 38.47°, 44.74°, 65.13°, 78.23°, and 82.43° correspond to the (111), (200), (220), (311), and (222) planes, of aluminum (ICDD 04-0787 chart). The different experimental conditions, such as substrate temperature and deposition time produce differences in the intensity of these peaks, which may be due to coating thickness or to the reduction of crystallite size of La_2O_3, or both, specially observed in the (002) plane for the hexagonal structure. That is, La_2O_3 coatings reduce the peaks intensity of hexagonal close packing or body center cubic structures when the temperature of the substrate is increased from 80 °C to 200 °C. The differences can be probably explained by different nucleation mechanisms occurring at the different experimental conditions. As a function of experimental conditions, La_2O_3 as well as $LaAl_{11}O_{18}$ compounds can form. The base pressure in the vacuum chamber prior to the deposition of the films is low enough (6.66E−2 m Pa) to avoid humidity contamination. However, it is well known [13–16] that La_2O_3 compounds are very reactive under ambient conditions. Thus, it is possible that the hydroxide films that are consistent with the XRD patterns were formed after the samples were exposed to the atmosphere.

In order to observe the substrate effect on the morphology of the films, the SEM micrographs of the as-growth CeO_2 and La_2O_3 coatings on the metallic substrates are shown in Fig. 3. To determinate a contrast in the surface morphologies, the samples are shown at the same magnification (50,000×). In general, all the as-deposited sputtered films have a uniform, crack-free, densely packed surface with small pores and smooth domes covering the substrate uniformly. These films were grown with clusters of nanosized cerium and lanthanum oxides particles. It is known that by changing the power, the sputter rate of the target changes resulting in differential deposition rates [17]. In addition, microstructural variations observed for the different operating conditions: the particle size changed from fine to coarse grain and the thicknesses varied from ~10 to 1200 nm, depending on the experimental conditions. Under these conditions, surface defects are not observable for cerium oxides, whereas the small surface cracks can be seen in some small areas of the La_2O_3 coatings.

To evaluate the influence of deposition parameters on the formation of different cerium and lanthanum oxides XPS analyses were carried out for the coatings. Selected as-deposited coatings for each rare earth deposited on silicon are shown in Fig. 4a–d. Over all for the sputtered Ce coatings, cerium was present in the Ce^{4+} and Ce^{3+} states. The Ce 3d spectrum is composed of five groups of spin-orbit splitting coupled peaks; in agreement with Burroughs and co-workers [18]. The effects of orbital hybridization are observed in the Ce 3d spectra which accounts for three doublets in Ce^{4+} (the main photoemission peaks and two satellites) and the two doublets in Ce^{3+} (the main peak and a satellite). The

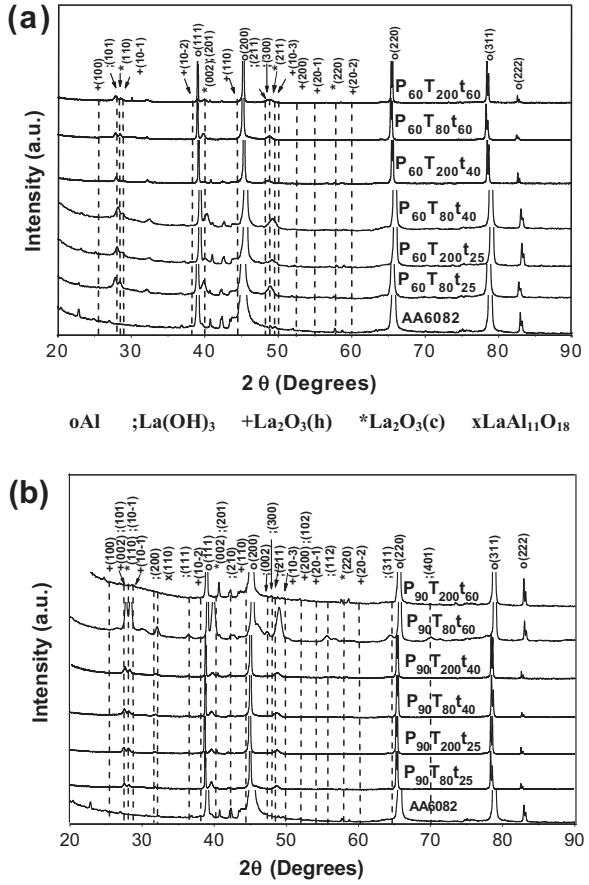

Fig. 2. X-ray diffraction patterns for La_2O_3 coatings onto AA6082 using different deposition parameters at two different powers: (a) 60 W and (b) 90 W.

Ce 3d spectrum consists of a 10-peak set, organized in 5 doublets corresponding to the 3d5/2 and 3d3/2 components (Fig. 4a and b). Three doublets, can be attributed to Ce^{4+} and are labelled as Ce^{4+} (at 886.75 and 904.35 eV, respectively), satellite Ce^{4+} (890.22 and 908.78 eV) and (899.43 and 917.3 eV), whereas the other two doublets corresponds to Ce^{3+} (883.48 and 902.04 eV) and its satellite Ce^{3+} (887.76 and 906.78 eV) [19]. The Ce^{4+} peak at 917.3 eV, which is exclusive of Ce^{4+} compounds and relatively well isolated from the rest of the spectrum, is commonly used as a valence state analysis of cerium compounds because its area is related to the total concentration of Ce^{4+} present in cerium coatings. The Ce^{3+}/Ce^{4+} ratio in the film is about 0.68. Hence, cerium in these oxides is primarily in the Ce^{4+} state.

The XPS-spectra for La and O are shown in Fig. 4c and d. The La 3d spectra also show one doublet. The peak positions obtained after peak fitting at 853.18 and 836.40 eV are for La^{3+} and at 857.68 and 840.93 eV for its satellite La^{3+}, in agreement with previous reports [20]. The oxygen 1s peak shows more than one component, suggestive of lanthanum hydroxide and oxide in similar concentrations. This suggests that during deposition lanthanum initially forms La_2O_3, and then upon exposure to the atmosphere reacts with moisture to form $La(OH)_3$.

3.3. Polarization curves

The modern theory of aqueous metallic corrosion is now based firmly on electrode kinetics [21–24]. Thus, in order to evaluate the anticorrosion properties of these sputtered films, the electrochemical determination of the kinetic parameters of as-deposited coatings were estimated using potentiodynamic polarization curves. Fig. 5a–d shows selected polarization curves for these coatings formed under different conditions at a san rate of 0.5–0.5 mV s^{-1}. The anodic polarization curves of uncoated aluminum AA6082 can be divided into two regions. In the first region, the dissolution of the AA6082 aluminum alloy occurs above its open circuit potential because an active electrochemical reaction takes place on the surface and the anodic current increases rapidly between −0.76 and −0.42 V vs. SCE. In a subsequent step, there is a passivation region beginning at this potential of −0.42 V vs. SCE. The rapid increase in the current density in the transpassivity zone indicates the occurrence of the stable pitting in which the potential corresponding to the current transient is known as a critical potential E_{pit} = −0.70 V vs. SCE. Finally, after the pit potential, it can be observe a tendency to the repassivation of microsize pits [25]. It is known that during the growing process of an occluded pit, the concentration of metallic cations increase gradually due to the active dissolution within the pit [26–28]. Once the saturated concentration is reached, a salt film will be formed at the bottom of the pit. The dissolved metallic cations move outward through the salt film under the action of electric field across the film. The stronger the field is, the faster the metallic cations move through the film. Hence, in this stage the growth of the pit is controlled by the ohmic potential drop across the salt film. The pitting corrosion occurs at the surface of aluminum alloy if a difference of −450 mV in positive direction is applied; however lower voltage differences contributed to achieving its passivity.

In the case of samples coated with cerium oxides, only the as-deposited samples at $P_{60}T_{80}t_{40}$ have a tendency to form a passivating film in the range from −0.86 to −0.59 V vs. SCE and display the lowest current density. The behaviour is followed by a rapid increase in the current density with a pitting potential varying from −0.59 to −0.44 V vs. SCE. The trend to the repassivation of microsize pits began from −0.44 V vs. SCE. It is evident that the pitting potential is modified is slightly shifted in positive direction when ceria coating is applied onto the metallic substrate using both deposition powers (60 and 90 W). On the other hand, in these plots (see Fig. 5a and b), the cathodic branch (at 60 W) remains practically the same for all of the coated specimens; whereas using a sputtering power of 90 W, a pronounced effect on the cathodic and anodic branches of the polarization curves can be clearly ob-

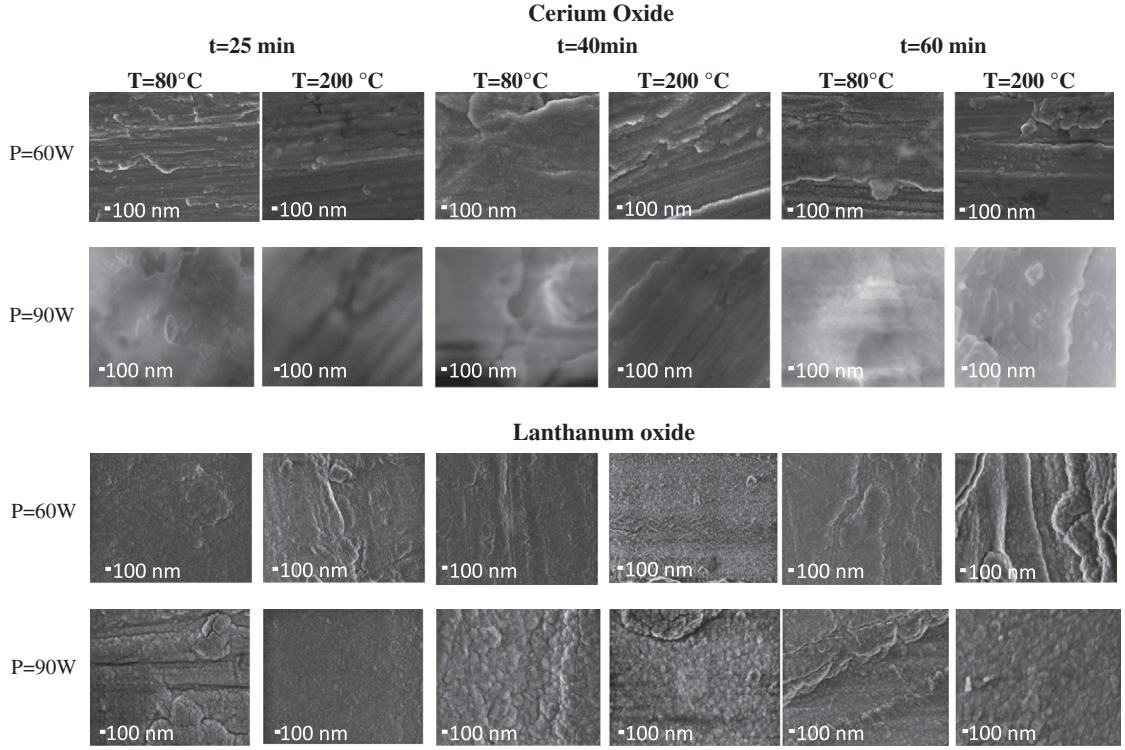

Fig. 3. SEM images at 50,000× showing the morphology of sputtered cerium and lanthanum oxides on AA6082 aluminum alloy using different experimental conditions.

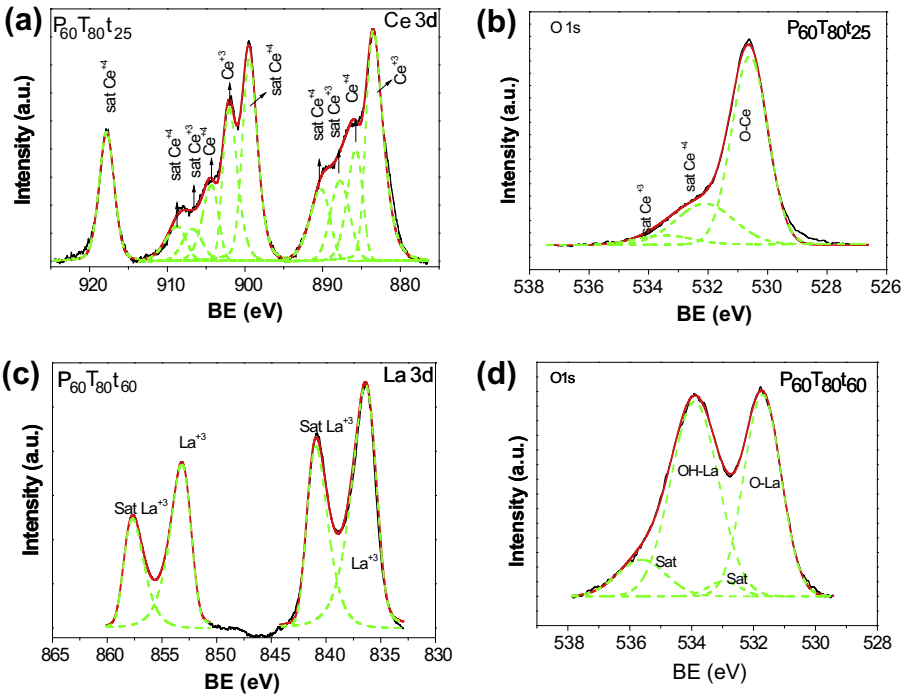

Fig. 4. High-resolution XPS spectra for Ce 3d (a and b) and for La 3d (c and d) deposited on the surface of selected samples.

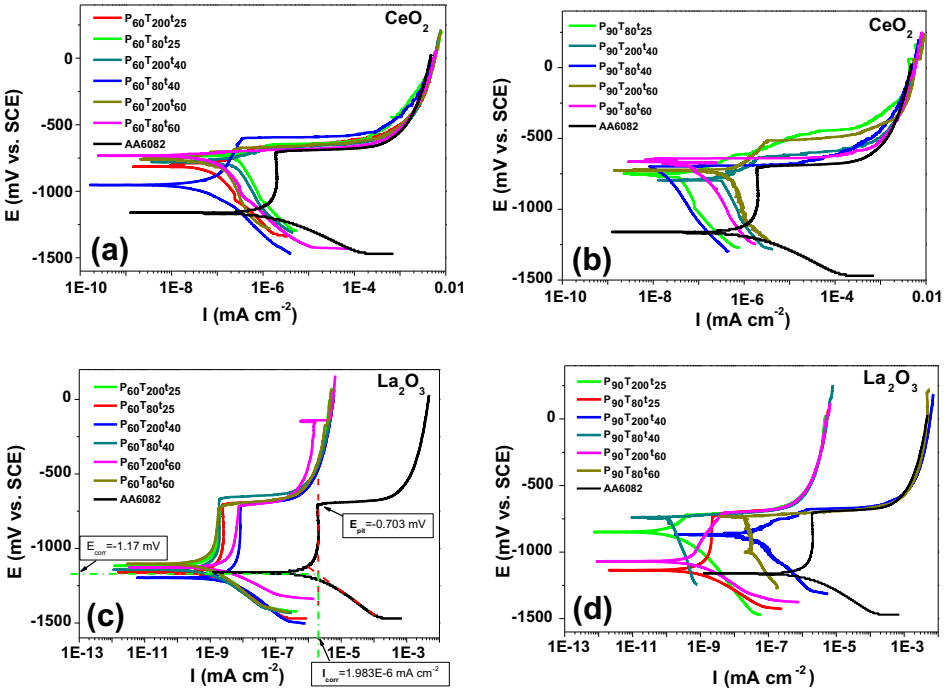

Fig. 5. Potentiodynamic curves corresponding to AA6082 aluminum alloy coated with cerium oxide (a and b) and lanthanum oxide (c and d) for various deposition parameters.

served; i.e. a limiting current density began to appear in the plots. Cathodic polarization drives the reduction reaction that in neutral sodium chloride solution is essentially the reduction of dissolved oxygen; thus inhibition of the reduction reaction is associated with the decrement of the dissolved oxygen. This behaviour indicates a change in the corrosion mechanism of the coated aluminum alloy. Unlike the situation with the uncoated alloy, there is an important inhibition of corrosion when RE are deposited modifying the rate determining step. Under the experimental conditions, the corrosion potentials are slightly shifted to nobler values depending on the conditions in the sputtering chamber. As a consequence, the passive stage is also shifted because E_{corr} is displaced. The alteration in the corrosion potential has been attributable to the ceria layer.

A rather low passivation current density can be reached in the polarization behaviour of the sputtered lanthanum oxide compounds on metallic substrates, which indicates that lanthanum coatings indeed can provide a better physical barrier to inhibit

Table 2
Fitting parameters of potentiodynamic curves of cerium and lanthanum oxides coated samples.

Sample	I_{corr} (A cm^{-2})	E_{corr} (V vs. SCE)	b_a (V dec.$^{-1}$)	b_c (V dec.$^{-1}$)	Sample	I_{corr} (A cm^{-2})	E_{corr} (V vs. SCE)	b_a (V dec.$^{-1}$)	b_c (V dec.$^{-1}$)
AA6082	1.98E−06	−1.17E00	–	0.143	–	–	–	–	–
CeO_2					*La_2O_3*				
$P_{60}T_{200}t_{25}$	5.76E−08	−8.09E−01	0.122	0.305	$P_{60}T_{200}t_{25}$	2.11E−06	−1.12E+00	–	0.207
$P_{60}T_{80}t_{25}$	3.18E−07	−7.31E−01	0.096	–	$P_{60}T_{80}t_{25}$	7.54E−06	−1.20E+00	–	0.215
$P_{60}T_{200}t_{40}$	2.47E−07	−7.79E−01	0.123	0.271	$P_{60}T_{200}t_{40}$	4.72E−06	−1.14E+00	–	0.286
$P_{60}T_{80}t_{40}$	1.18E−08	−9.55E−01	–	–	$P_{60}T_{80}t_{40}$	4.59E−06	−1.13E+00	–	0.148
$P_{60}T_{200}t_{60}$	4.17E−08	−1.06E+00	–	0.187	$P_{60}T_{200}t_{60}$	6.56E−08	−7.55E−01	–	0.304
$P_{60}T_{80}t_{60}$	8.06E−08	−7.33E−01	0.104	–	$P_{60}T_{80}t_{60}$	5.06E−06	−1.16E+00	–	0.229
$P_{90}T_{80}t_{25}$	4.20E−08	−7.52E−01	0.095	–	$P_{90}T_{200}t_{25}$	1.08E−07	−8.47E−01	–	0.228
$P_{90}T_{200}t_{40}$	4.72E−07	−7.95E−01	0.168	–	$P_{90}T_{80}t_{25}$	2.12E−06	−1.14E+00	–	0.201
$P_{90}T_{80}t_{40}$	2.96E−07	−6.96E−01	0.118	–	$P_{90}T_{200}t_{40}$	2.85E−08	−8.69E−01	–	0.232
$P_{90}T_{200}t_{60}$	4.89E−07	−7.26E−01	0.197	–	$P_{90}T_{80}t_{40}$	1.81E−07	−7.39E−01	–	–
$P_{90}T_{80}t_{60}$	5.80E−08	−6.54E−01	0.136	–	$P_{90}T_{200}t_{60}$	1.79E−08	−7.29E−01	–	–
					$P_{90}T_{80}t_{60}$	7.04E−07	1.07E+00	–	0.141

the electrochemical process (Fig. 5c and d). The deposition of lanthanum coatings maintaining the power at 60 W, varying the deposition time and substrate temperature seems to shift the passivity towards to more positive values, whereas no trend can be reasonable analysed with deposited samples using lanthanum oxide target at 90 W; in this situation is regarded that for some samples, it is exhibited a poor resistance to localized corrosion because the coatings are non-passive.

Table 2 shows the kinetic parameters from corrosion testing indicating the effects of the various deposition parameters. The values of I_{corr} and E_{corr} were obtained as an approximation by extrapolating the fitting lines of the anodic and cathodic branch back to E_{ocp}, respectively. It is important to note that only Tafel slopes with a physical significance were calculated. Assuming that the corrosion rate is proportional to the corrosion current density (I_{corr}), the Lanthanum (90 W, 200 °C, 60 min)-coated specimens have the lowest I_{corr} (1.79E−8 A cm^{-2}) with a high resistance against pitting corrosion failure (E_{pit} = −0.68 V). The alteration in the corrosion potential has been attributable to the dense or porous layer that grows on metallic substrate and also its behaviour in chloride solution, therefore, the potential corresponds to a mixing potential that is influenced by the interaction between the Al_2O_3 film and Lanthanum compounds. It is recognized that this process could also be responsible of the sealing, adhesion, and increase the anticorrosion properties against of these coatings. Comparing both RE sputtered coatings, potentiodynamic curves and kinetic parameters confirmed that Lanthanum oxide coatings resulted in enhanced in the shifting of pitting potential and corrosion current density compared to ceria coatings with maximum increase observed at the experimental conditions of $P_{90}T_{200}t_{60}$ and $P_{60}T_{80}t_{40}$, respectively. It can be also concluded that such electrochemical performance is greater as increase the deposition time in the sputter chamber. Finally, the performance can be correlated with the fact that La oxides/hydroxides are surface-active films forming a dense and uniform oxide/hydroxide layer, which can inhibit the diffusion of Cl^- ions and thus delay the oxidation and corrosion process.

4. Conclusions

This paper describes the deposition parameters effects of power, substrate temperature, and deposition time for sputtered rare earth coatings on the corrosion behaviour of AA6082 aluminum alloy immersed in aqueous solutions of NaCl. These three process parameters affect the microstructure and chemistry of the Ce and La oxides/hydroxides formed by sputter deposition on different substrates. The deposition rate increase with the power from 60 W to 90 W, but a slight drop in the deposition rate can be seen with the substrate temperature. Maintaining constant the power and substrate temperature during the experimental set up, it was observed that the deposition time had an adverse effect on the thickness of both rare earth coatings.

Interesting changes are observed by increasing the substrate temperature modifying the crystallinity of the rare earth coatings. XRD and XPS findings demonstrate that the cerium coatings are composed of CeO_2 and a significant quantity of Ce_2O_3 due to the oxygen deficiency in the sputtering chamber, whereas La_2O_3 and some intermetallic La compounds ($LaAl_{11}O_{18}$) are mainly detected in lanthanum layers. In addition, in the surface and sub-surface layers $La(OH)_3$ compounds are apparently formed after exposure of La_2O_3 thin films due to its very reactive with the environment. The structure of these coatings is found to be dependent on the nature of the substrate. Under similar conditions, the thicknesses of the La-coatings are greater than those of the cerium coatings which directly affect the corrosion protection; i.e. a rather low current density (1.79E−08 A cm^{-2}) can be reached in the polarization behaviour of the sputtered lanthanum oxide compounds on metallic substrates, indicating that lanthanum coatings indeed can provide a better physical barrier to inhibit the electrochemical process.

Acknowledgements

The authors acknowledge the financial support provided by CONACYT through the 133618 and 132660 Projects, PAPIIT 103910, SIP-IPN 2014-0164, 2014-0992 SNI-CONACYT and COFAA-IPN. S.B. Brachetti Sibaja is grateful for a Postgraduate fellowship from SIP-IPN. The authors also thank M.Ed. Adela, E. Rodríguez Salazar and Q.I. Ana Cecilia Espíndola Flores for technical support.

References

[1] H. Schâfer, H.R. Stock, Corros. Sci. 47 (2005) 953–964.
[2] S.P. Knight, M. Salagaras, A.R. Trueman, Corros. Sci. 53 (2011) 727–734.
[3] K. Seong-Jong, H. Min-Su, K. Seong-Kweon, J. Seok-Ki, T. Nonferr. Metal Soc. 21 (2011) s17–s22.
[4] W. Zhang, B. Hurley, R.G. Buchheit, J. Electrochem. Soc. 149 (2002) B357–B365.
[5] M.W. Kendig, R.G. Buchheit, Corrosion 59 (2003) 379–400.
[6] P. Schmutz, G.S. Frankel, J. Electrochem. Soc. 146 (1999) 4461–4472.
[7] H. Sun, H. Wang, F. Meng, J. Rare Earths 29 (2011) 991–996.
[8] T.P. Schuman, Protective coatings for aluminum alloys, in: Myer Kutz (Ed.), Handbook of Environmental Degradation of Materials, William Andrew, Inc., USA, 2005, pp. 345–366.
[9] B.A. Shaw, G.D. Davis, T.L. Fritz, B.J. Rees, W.C. Moshier, J. Electrochem. Soc. 138 (1991) 3288–3295.
[10] M.A. Domínguez-Crespo, A.M. Torres-Huerta, S.E. Rodil, E. Ramírez-Meneses, G.G. Suárez-Velázquez, M.A. Hernández-Pérez, Electrochim. Acta 55 (2009) 498–503.
[11] G. Bräuer, B. Szyszka, M. Vergöl, R. Bandorf, Vacuum 84 (2010) 1354–1359.

[12] C.Y. Lin, D.Y. Lee, S.Y. Wang, C.C. Lin, T.Y. Tseng, Surf. Coat. Technol. 203 (2008) 480–483.
[13] B.F. Rivera, B.Y. Jhonson, M.J. O'Keefe, W.G. Fahrenholtz, Surf. Coat. Technol. 176 (2004) 349–356.
[14] M. Nieminem, M. Putkonen, L. Ninistö, Surf. Sci. 174 (2001) 155–166.
[15] N. Imanaka, T. Masui, Y. Kato, J. Solid State Chem. 178 (2005) 395–398.
[16] C. Yang, H. Fan, Y. Xi, S. Qiu, Y. Fu, Thin Solid Films 517 (2009) 1677–1680.
[17] M. Ohring, The Materials Science of Thin Films, second ed., Academic Press, San Diego (CA), 1991.
[18] P. Burroughs, A. Hammett, A.F. Orchard, G. Thornton, J. Chem. Soc., Dalton Trans. 17 (1976) 1686–1698.
[19] J.M. Sánchez-Amaya, G. Blanco, F.J. Garcia-Garcia, M. Bethencourt, F.J. Botana, Surf. Coat. Technol. 213 (2012) 105–116.
[20] A. Pardo, S. Feliú Jr., M.C. Merino, R. Arrabal, E. Matykina, Appl. Surf. Sci. 254 (586) (2007) 586–595.
[21] J.A.V. Butler, Trans. Faraday Soc. 19 (1924) 734–739.
[22] T. Erdey-Gruz, M. Volmer, Z. Phys. Chem. 150 (1930) 203–213.
[23] C. Wagner, W. Traud, Z. Elektrochem. 44 (1938) 391.
[24] J. Tafel, Z. Phys. Chem. 50 (1905) 641–712.
[25] M. Mandel, L. Krüger, Corros. Sci. 73 (2013) 172–180.
[26] V. Moutarlier, M.P. Gigandet, J. Pagetti, Appl. Surf. Sci. 206 (2003) 237–249.
[27] Z. Szklarska-Smialowska, Corros. Sci. 41 (1999) 1743–1767.
[28] A.G. Muñoz, J.B. Bessone, Corros. Sci. 41 (1999) 1447–1463.